JOURNAL OF VIROLOGY, Feb. 2009, p. 1941–1951 Vol. 83, No. 4
0022-538X/09/$08.00+0 doi:10.1128/JVI.01752-08

Leader-Induced Phosphorylation of Nucleoporins Correlates with Nuclear Trafficking Inhibition by Cardioviruses[▽]

Frederick W. Porter* and Ann C. Palmenberg

Institute for Molecular Virology and Department of Biochemistry, University of Wisconsin-Madison, Madison, Wisconsin 53706

Received 19 August 2008/Accepted 3 December 2008

Picornaviruses disrupt nucleocytoplasmic trafficking pathways during infection. Poliovirus and rhinovirus inhibit nuclear protein import/export through a series of 2A protease-dependent cleavages within nuclear pore proteins (nucleoporins [Nups]), including Nup62, Nup98, and Nup153. Cardioviruses lack the same protease and instead affect trafficking inhibition through an activity mapped to their leader (L) protein, a 67- to 76-amino acid (aa) polypeptide with no known enzymatic activity. We have shown that L from encephalomyocarditis virus (EMCV) binds and inhibits the activity of Ran-GTPase, a key regulator of nucleocytoplasmic transport. We now report that recombinant EMCV L triggers the unregulated efflux of protein cargo from preloaded HeLa cell nuclei in cell-free reactions dependent upon *Xenopus* egg cytosol or HeLa cell-derived cytosol. Recombinant L was the only viral protein necessary for this activity or for nuclear protein import inhibition. Mutational disruption of the L protein zinc finger domain ($C_{19}A$) abrogated the inhibitory activity for both import and efflux in cell extracts, but mutations in the C-terminal acidic domain of L (aa 37 to 61) did not. Notably, HeLa cell nuclei treated with L, or those from EMCV-infected cells, showed reproducibly altered patterns of nucleoporin phosphorylation. Nup62, Nup153, and Nup214 each became hyperphosphorylated in an L-dependent manner. Staurosporine, a broad-spectrum kinase inhibitor, blocked this phosphorylation and rescued nuclear import/export activity from L-dependent inhibition. Therefore, cardioviruses target the same group of nucleoporins as enteroviruses, but the effector mechanism triggered by L (or L-Ran complexes) involves a unique cytosol-dependent phosphorylation cascade rather than proteolysis.

Nuclear pore complexes (NPCs) are massive proteinaceous structures spanning the nuclear envelope and enabling the regulated trafficking of protein and RNA between the cytoplasm and nucleus (31). The NPCs of higher eukaryotes are assembled from about 30 different integral proteins, called nucleoporins (Nups), arranged with eightfold radial symmetry (33). The specificity of protein movement into or out of a nucleus depends on a cargo's display of a nuclear localization signal (NLS) or a nuclear export signal (NES), which mediates docking with requisite transport receptors (10, 19). Receptor-cargo complexes traverse the NPC via transient interactions with phenylalanine-glycine (FG) repeat domains on Nups lining the central channel of NPC (32, 34). Active transport is regulated by the small GTPase, Ran, which exists predominantly in a GDP (cytoplasm) or GTP (nucleus) format on respective sides of the NPC (1, 11). Since cargo receptors have different affinities for Ran-GDP versus Ran-GTP, the NPC-imposed gradient efficiently orchestrates the loading of cargo on one side of the pore and unloading on the other (12). If the Ran gradient is disrupted, active import/export is inhibited, although proteins smaller than about 40 kDa may still shuttle back and forth by passive diffusion (25).

Cellular gene expression and activation of innate immunity pathways are absolutely dependent on signals traversing the NPC, so it is not surprising that many viruses commandeer the canonical transport processes for their own benefit. The lack of active import can help relocalize beneficial nuclear-targeted proteins to new sites on the Golgi apparatus or endoplasmic reticulum (13), where they may be usurped for viral translation or RNA synthesis. In addition, the inhibition of active trafficking can block the nuclear import of antiviral signals or prevent the export and availability of cellular mRNAs detrimental to virus processes. A well-known example is that the matrix protein of vesicular stomatitis virus binds simultaneously to Nup98, a component of the NPC, and to the transport factor Rae1. The new protein complex prevents the export of cellular mRNA, snRNA, and snRNPs (7, 37), thereby stalling cellular gene activation and the triggering of antiviral activities (17).

RNA viruses in the *Picornaviridae* family also disrupt the normal movement of cellular proteins and RNA across the nuclear envelope during infection, although viruses in each genus of this family use a different requisite component(s) and mechanism(s) to achieve their effects. For the enteroviruses (e.g., poliovirus and rhinovirus), a virus-encoded protease, 2A, cleaves and disrupts the activities of several FG nucleoporins, including Nup62, Nup98, and Nup153 (14, 15, 27). As a result, the receptors for many cellular cargos cannot transit the NPCs, regardless of their directional signal sequences (e.g., NES and NLS). Other cellular proteins normally retained in the nucleus redistribute to the cytoplasm as a consequence of altered NPC permeability, and several of these (e.g., Nucleolin, PTB, Sam68, and La autoantigen) are subsequently captured in RNA-protein complexes for use during the virus replication cycle (13).

Picornaviruses in the *Cardiovirus* genus, such as encephalomyocarditis virus (EMCV) and Theiler's murine encephalomyelitis virus, also have inhibitory trafficking phenotypes, although they lack a 2A-like protease and none of the NPC Nups

* Corresponding author. Mailing address: Institute for Molecular Virology, Robert Bock Laboratories, University of Wisconsin-Madison, 1525 Linden Dr., Madison, WI 53706. Phone: (608) 262-7228. Fax: (608) 262-6690. E-mail: fwporter@wisc.edu.

▽ Published ahead of print on 10 December 2008.

TABLE 1. Primer sequences

Primer no.	Sequence
972	5′-CGAGCATTCCTAGGGGTCTTTCCC-3′
973	5′-CTCCTCTGGGAACCATTCTTC-3′
974	5′-GAATGGTTCCCAGAGGAGTTATTG-3′
975	5′-ACACTCGATCAGACAGATTCTCCA-3′
999	5′-AGAGCATTTTGGGGCTTCCTCAAAAGTGAG-3′
1000	5′-GAGGAAGCCCCAAAATGCTCT-3′
1008	5′-AAAGGATCCATGGCCACAACCATGGAACAAGAG-3′
1033	5′-TTATTGGCTGATGGAGAGGATGATGTC-3′
1034	5′-CTCTCCATCAGCCAATAACTCCTCTGG-3′
1062	5′-GGAATTCACTACTGTAACTCGAAAACGACT-3′

are cleaved during infection (20). These viruses instead regulate nuclear trafficking through a 67-amino-acid (EMCV) or 76-amino-acid (Theiler's murine encephalomyelitis virus) leader (L) protein with an unusual N-terminal zinc finger protein-binding motif and a C-terminal acidic domain (5, 20). We have reported that recombinant EMCV L binds tightly to Ran-GTPase, the molecular switch which drives both nuclear import and export pathways (30). The presence of L inhibits normal Ran function in cell-free mitotic spindle assembly reactions, and the expression of L within cDNA-transfected cells is sufficient to inhibit cellular mRNA export from nuclei. Mutations engineered into the L zinc finger domain, which disrupt Ran binding, are also ineffective viral sequences for trafficking shutoff. During infection with wild-type EMCV, the disruption of nucleocytoplasmic trafficking is observed as a very early event. It occurs within 2 to 3 h postinfection (p.i.), even before the onset of viral replication. At such early times, the cellular concentration of Ran far exceeds that of L, and therefore, the virus-triggered NPC modulation function cannot be strictly stoichiometric. Rather, in addition to a Ran-binding function, a few copies of L must be able to leverage their effects through an alternate or parallel indirect inhibition mechanism.

We have now characterized alterations in the NPC proteins induced by EMCV infection and identified those which are dependent upon the activity of the L protein in isolation. We report here that several FG repeat Nups became hyperphosphorylated in an L-dependent manner as long as the reaction mixtures also contained added cytosol as the source of the requisite kinase(s). Nup phosphorylation was observed under every condition of L-directed inhibition of nuclear import/efflux, indicating that this phenomenon is essential to L protein function.

MATERIALS AND METHODS

Cells and viruses. Plasmid pEC_9-L_{C19A}, encoding infectious EMCV with a point mutation in the zinc finger of L, was constructed by two-step PCR. *Pfu* polymerase (Stratagene), mutagenic primers (999 and 1000) (Table 1), and subsequent flanking primers (972 and 975) (Table 1) amplified and altered the L-coding region from pEC_9 cDNA (16). The resulting amplicon was ligated back into pEC_9 using AvrII and NheI restriction sites.

HeLa cells (ATCC CRL-1958) were grown (37°C; 5% CO_2) in modified Eagle's medium supplemented with 10% calf serum. Recombinant virus, vEC_9 or vEC_9-L_{C19A}, was cultured after transfection of cell monolayers with RNA transcripts (6). Human rhinovirus type 16 (HRV-16; ATCC VR-283) was a kind gift of Wai-Ming Lee. Infection of confluent HeLa cell monolayers at the designated multiplicity of infection (MOI) for all viruses was as described previously (30).

Recombinant proteins. Plasmid pGST-GFP_{NLS} has been described previously (24). It carries fused genes for green fluorescent protein (GFP) and glutathione *S*-transferase (GST), linked to a simian virus 40 large T-antigen NLS. Expression in transformed *Escherichia coli* DH5α (bacterial) cells was induced with isopropyl-β-D-thiogalactoside (1 mM). Cell extracts were prepared after treatment with lysozyme (0.5 mg/ml in 25 mM Tris-HCl, pH 7.4, 150 mM NaCl, 5% glycerol, 1 mM dithiothreitol [DTT], 1 mM phenylmethylsulfonyl fluoride) and sonication. Soluble recombinant protein was isolated after extract clarification, using glutathione-Sepharose high-performance resin (GE Healthcare), and then dialyzed (20 mM HEPES, pH 7.3, 110 mM potassium acetate) before purity (sodium dodecyl sulfate-polyacrylamide gel electrophoresis [SDS-PAGE]) and concentration (Bradford kit; Bio-Rad) were assayed.

Plasmids for bacterial expression of EMCV L proteins (pGST-L, pGST-L_{C19A}, pGST-$L_{\Delta a}$), fused to amino-terminal GST tags and His_6-tagged human Ran (pHisRan) have been described previously, as have protocols for protein purification (4, 30). Additional L configurations (pGST-L_{T47A} and pGST-L_{Y41F}) were constructed in two-step PCRs with *Pfu* polymerase, mutagenic primer pairs ($T_{47}A$, 1033 and 1034; $Y_{41}F$, 974 and 973) and flanking primers (1008 and 1062) using the L-coding region of pEC_9 as a template (Table 1). The resulting amplicons were ligated into pGEX-6-P DNA (GE Healthcare) after digestion of the plasmid and insert(s) with BamHI and EcoRI. Transformation, induction, protein isolation, purity, and concentration assessments were the same as those for GST-GFP_{NLS}.

Reporter tracking during infection. Nuclear reporter plasmid, pHT_{3NLS}, fused the full-length HaloTag gene to three tandem copies of the simian virus 40 large T-antigen NLS sequence. The plasmid backbone was derived from pAcGFP1-nuc (BD Biosciences) by removing the GFP-coding region (digestion with NheI and BspEI) and replacing it with a HaloTag-coding fragment from pHT2 (Promega), digested with NheI and NgoMIV. HeLa cells (50% subconfluent monolayers in 24-well plates) were transfected with pHT2 (Promega) or pHT_{3NLS} using Lipofectamine 2000 (Invitrogen) according to the manufacturer's recommendations (typically, 0.4 μg cDNA per well was used). The cells were cultured for 24 h (5% calf serum, Opti-MEM I medium; Invitrogen) to allow protein expression under the transcriptional control of a cytomegalovirus immediate-early promoter endogenous to each plasmid. The medium was replaced with Opti-MEM I containing HaloTag TMR ligand (5 μM; Promega). After incubation (25 min at 37°C), the cells were washed (three times) with warm phosphate-buffered saline and then infected with vEC_9 (MOI = 50). Between 1 and 5 h later, the cells were washed again and the TMR signal was visualized (Nikon TE2000S fluorescence microscope with ×20 objective and the tetramethyl rhodamine isothiocyanate [TRITC] filter set) or harvested and denatured prior to protein fractionation by SDS-PAGE. TMR-labeled HaloTag bands were detected with a Typhoon 9200 imager (GE Healthcare) equipped with a 532-nm excitation laser and 580-nm band-pass 30 emission filter.

Reporter tracking in digitonin-treated cells. Interphase *Xenopus* egg extracts (26) were clarified (16,100 × *g* for 15 min at 4°C) before the soluble fraction was snap-frozen (liquid nitrogen) into single-use aliquots. Nuclear import assays were similar to those described previously (1). Briefly, HeLa monolayers (60% confluent, using 12-mm coverslips in 24-well dishes) were washed once with transport buffer (TB; 20 mM HEPES, pH 7.3, 110 mM potassium acetate, 2 mM magnesium acetate, 1 mM EGTA, 2 mM DTT at 4°C), permeabilized with digitonin (20 μg/ml), and then washed again with TB. Individual import mixtures (TB containing 50% *Xenopus* egg extract, 1 mM ATP, 0.5 mM GTP, 75 μg/ml GST-GFP_{NLS}) including the desired effectors (i.e., wheat germ agglutinin [WGA; 5 μg/reaction; Sigma], GST, GST-L, or GST-L_{C19A}) were assembled on ice and then placed as droplets (40 μl) onto Parafilm. Reactions were initiated by inverting cell-covered coverslips onto the droplets. After incubation (20°C in the dark for 35 min), TB was added (400 μl at 4°C) before the coverslips were washed (twice with TB), fixed (4% formaldehyde), and then mounted on microscope slides (Vectashield mounting medium; Vector Labs). Nuclear efflux assays omitted the effector protein from the initial import mixtures. After the coverslips were incubated and washed (twice with TB), they were reinverted onto fresh droplets of new import mixtures, this time containing the desired effectors. Incubation, washing, fixing, and mounting were the same as for import assays.

When appropriate, the cell samples were treated with monoclonal antibody 414 (MAb 414; Covance) and TRITC-conjugated goat anti-mouse immunoglobulin G (IgG; Sigma) as primary and secondary antibodies, respectively. DNA was stained with DAPI (4′,6-diamidino-2-phenylindole; 0.5 μg/ml) during secondary

antibody incubation. The mounted samples were visualized with a Nikon Eclipse TE2000U laser confocal microscope (×60/1.4 PlanApo objective). Signals for GFP, TRITC, and DAPI used 488-, 543-, and 405-nm-wavelength lasers, respectively, in independent series. Within each experiment, all images were acquired with identical settings. Imaged signals for nuclear GST-GFP_{NLS} were assigned relative values by measuring the pixel density (ImageQuant software) within circles of identical dimensions for 20 representative nuclei. Averages and standard deviations were determined over several independent experiments. Linear scans of GFP (cargo) and Nup signals (MAb 414) for individual cells (ImageQuant) used grayscale images derived from respective collection channels. For accuracy and to reduce noise, the scans report the average pixel density within a sliding window (3 pixels in width by 21 pixels in height) as it moved across the image.

Western blot analyses. Rabbit polyclonal serum raised to the EMCV capsid was described previously (2). Primary reagents against tubulin (murine MAb, SC-5286; Santa Cruz Biotech), eIF-4G (rabbit polyclonal, SC-11373; Santa Cruz Biotech), GFP (rabbit polyclonal, SC-8334; Santa Cruz Biotech), lamin A (murine MAb, ab8980; Abcam), and FG-containing nucleoporins (murine MAb 414; Covance) were commercial, as were appropriate horseradish peroxidase-conjugated secondary antibodies (A2554 and A0545; Sigma).

Whole cells or digitonin-treated nuclei for protein analyses were washed (phosphate-buffered saline) and then harvested into lysis buffer (20 mM Tris, pH 7.6, 140 mM NaCl, 2.5 mM EDTA, 1% SDS [wt/vol], 1× phosphatase inhibitor cocktail 1; Sigma), sonicated, combined with gel loading buffer, and boiled. Nuclear and cytoplasmic fractions were separated by centrifugation (500 × *g* for 5 min), following cell lysis in hypotonic buffer (10 mM Tris, pH 7.4, 10 mM NaCl, 3 mM $MgCl_2$, 0.5% NP-40 [vol/vol], 1× phosphatase inhibitor cocktail 1), and then prepared for analysis as described above. After SDS-PAGE fractionation, the proteins were electrotransferred onto membranes (Immobilon P [Millipore] in 25 mM Tris, pH 8.0, 0.19 M glycine, 20% methanol), treated with blocking solution (20 mM Tris, pH 7.6, 140 mM NaCl, 0.05% Tween 20, 10% nonfat dry milk), rewashed (twice in Tris-buffered saline–Tween 20 [TBST; 20 mM Tris, pH 7.6, 140 mM NaCl, 0.05% Tween 20]), incubated with the primary antibody (in TBST with 1% nonfat dry milk at 4°C and for 12 h), and then washed again (three times in TBST) before treatment with secondary antibody (in TBST with 1% nonfat dry milk). After subsequent washes (three times in TBST), the membranes were exposed to film in the presence of enhanced chemiluminescence substrate (GE Healthcare).

Phosphoprotein analyses. Mock-infected or infected cell extracts, collected as described above, were diluted (1:10 in 20 mM Tris-Cl, pH 7.6, 340 mM NaCl, 2.5 mM EDTA, 1% Triton X-100, 1× phosphatase inhibitor cocktail 1), incubated on ice, and then clarified (16,100 × *g* for 15 min at 4°C) before the supernatants were reacted (3 h; 4°C) with MAb 414 or a control mouse IgG (SC-2025; Santa Cruz Biotech), immobilized on protein G-Sepharose beads (GE Healthcare). The beads were washed (three times in 50 mM Tris-Cl, pH 7.6, 340 mM NaCl, 2.5 mM EDTA, 0.1% Triton X-100) and then washed again with buffer (20 mM Tris-Cl, pH 7.6, 136 mM NaCl, 10 mM $MgCl_2$, 0.1 mM DTT) before incubation (30 min, 37°C) with 2.5 U calf intestinal phosphatase (NEB). Protein was removed from the beads by being boiled in loading buffer prior to SDS-PAGE fractionation and detection by Western blot analysis. For direct phosphoprotein detection, peppermint stick reference standards (Invitrogen) were included in parallel gel lanes. Gels were incubated in Pro-Q Diamond phosphoprotein stain (Invitrogen), and the signals were visualized with a Typhoon 9200 (GE Healthcare) imager equipped with a 532-nm excitation laser and 560-nm long-pass emission filter. All images were analyzed with ImageQuant software.

RESULTS

Virus-induced nuclear efflux. Prior observations with mengovirus- and EMCV-induced nuclear efflux monitored HeLa cells constitutively expressing enhanced green fluorescent protein-NLS or reporter redistribution after transient transfection with Timer-NLS protein vectors (20). We developed an alternate assay for early infection events, using HaloTag-expressing transfection vectors differing by the presence (pHT_{3NLS}) or absence (pHT2) of a tandem-linked NLS. When reacted with the cell-permeable TMR ligand, HaloTag gives a strong fluorescent snapshot of the existing protein location, and the long-lived signal (visual or quantitative) is easily tracked during a subsequent chase without label transfer to new proteins. In the absence of infection, HaloTag expressed from pHT2 distributed equivalently between the cytoplasm and the nucleus, showing the expected pattern for a small inert protein (33 kDa) subject to diffusion (Fig. 1A). The modified protein with an NLS (pHT_{3NLS}) was instead directed to the nucleus, where the pulse-labeled signal concentrated and was visible for at least 24 h in mock-infected cells (data not shown). Infection with vEC_9 did not immediately affect this signal. The reporter remained primarily nuclear for 2 to 3 h p.i., at which point individual cells began to relocate their fluorescence into the cytoplasm and rapidly took on an appearance similar to that of pTH2-transfected cells (Fig. 1C). Although it was difficult to catch specific cells in transition, by 3 to 4 h p.i. nearly all cells had undergone nuclear efflux and redistribution of their HaloTag. Once the reporter was dispersed, later infection points (up to 6 h p.i.) showed no further change in cell morphology or label distribution. HaloTag-ligand complexes are stable to SDS-PAGE. When parallel cell samples were fractionated, the fluorescent band patterns were identical (Fig. 1B) for at least 6 h p.i., confirming that infection had not detached the NLS linkage or triggered reporter degradation.

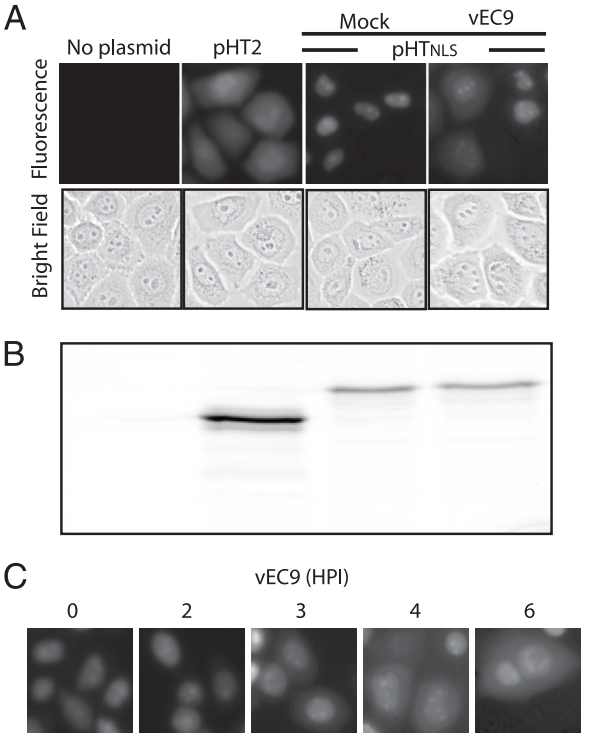

FIG. 1. EMCV promotes nuclear efflux. (A) HeLa cells were transfected with pHT2 or pHT_{NLS} cDNA. After 24 h, HaloTag-TMR ligand was added, and 30 min later, the cells were infected with vEC_9 (MOI = 50). Fluorescence microscope images of live cells were taken at 3 h p.i. (B) Parallel samples were lysed in SDS and fractionated by PAGE, and the TMR signals were localized by fluoroimaging. (C) Cells were transfected with pHT_{NLS} and then infected as described for panel A. Samples were imaged at the indicated times p.i.

Recombinant L inhibits nuclear import and induces nuclear efflux. EMCVs with mutations in the L protein zinc finger or acidic domains are defective in nuclear efflux assays during infection (20), but the assignment of L culpability was not achieved in the absence of other viral proteins. Digitonin-

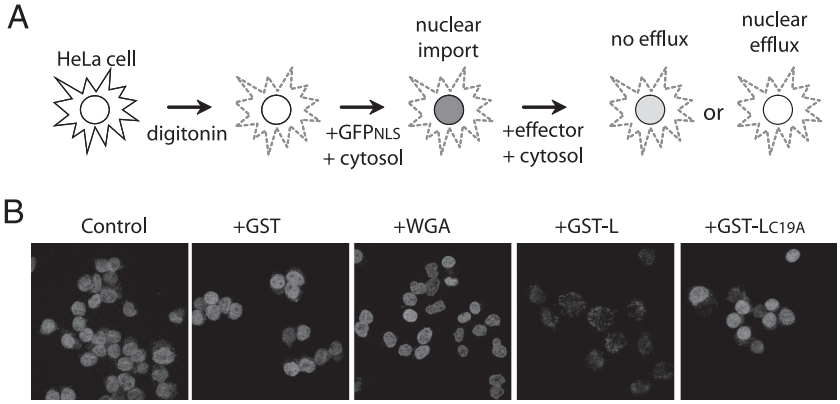

FIG. 2. Recombinant L protein promotes nuclear efflux. (A) Schematic of digitonin nuclear efflux assay. (B) Digitonin-treated HeLa cells were incubated with an import mixture containing *Xenopus* egg cytosol, ATP, GTP, and import substrate (GST-GFP_{NLS}). Cells were washed twice and then exposed to fresh import mixture lacking the reporter but containing the indicated effector (3 μM GST, GST-L, or GST-L_{C19A}) or WGA control. The cells were washed, fixed, and then visualized by confocal microscopy.

treated HeLa cells are permeable to added proteins. When presented with exogenous cytosol (e.g., *Xenopus* egg) and an energy source (ATP/GTP), nuclear import and export pathways are activated (1). Recombinant reporters displaying an appropriate NLS (i.e., GST-GFP_{NLS}) readily trafficked into these nuclei and accumulated (Fig. 2). After subsequent treatment with fresh cytosol containing recombinant GST-L, the labeled nuclei underwent reporter efflux just like infected cells. Even at room temperature (20°C), the presence of GST-L triggered nuclear depletion of at least 80% of the reporter signal within just a few minutes. Treatment with an inactive L protein (GST-L_{C19A}), GST alone, or WGA, a lectin known to inhibit nuclear import by binding nucleoporins (9), did not induce a similar signal loss. Therefore, L is the only viral protein necessary for this activity, and its mechanism is independent of the viral replication cycle.

Nuclear efflux of an NLS-encoding protein occurs when the rate of diffusion exceeds that of active import. The presence of EMCV L protein in cells or cell extracts clearly allowed diffusion to dominate through the treated NPC, but it was unclear whether L achieved this effect by inhibiting active import. Since uptake into digitonin-treated cells is easily synchronized, the

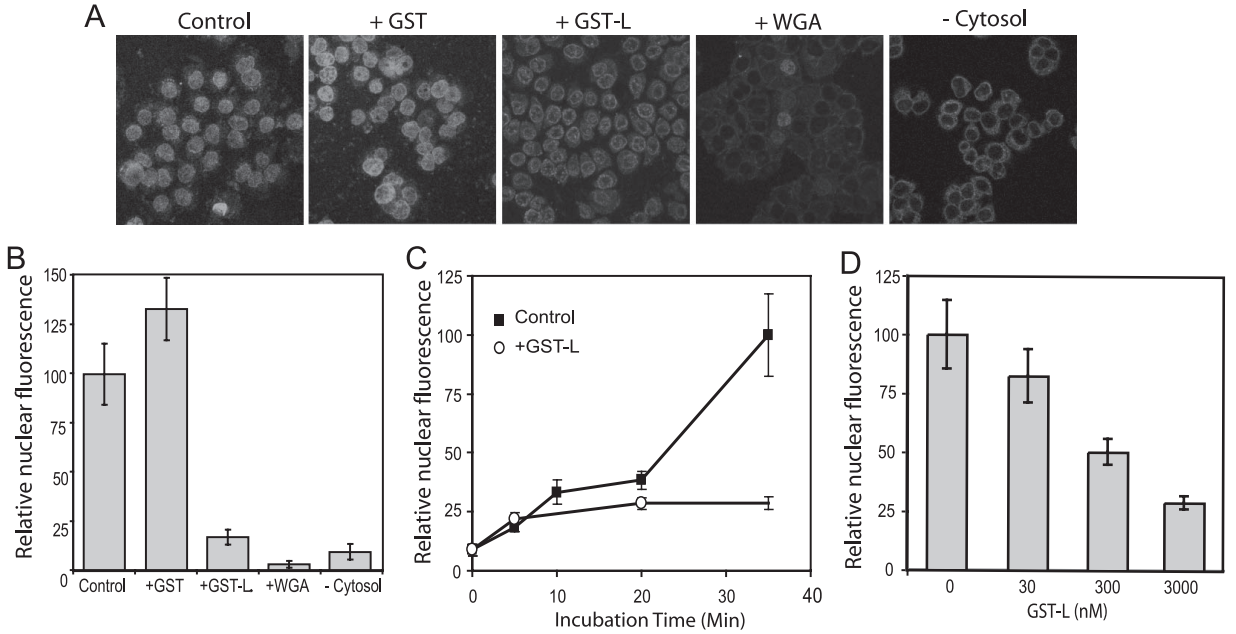

FIG. 3. Recombinant L protein inhibits nuclear import. (A) Similar to Fig. 2, digitonin-treated HeLa cells were reacted with import mixtures, except that the effectors and reporter (GST-GFP_{NLS}) were both included during the initial incubation (3 μM). After 35 min, the cells were washed, fixed, and visualized by confocal microscopy. (B) The confocal images were captured digitally, and the GFP-specific pixels from equivalent-area centers of 20 nuclei in representative fields were recorded. The average pixel density (relative nuclear fluorescence) in the absence of effectors (Control) was set at 100%. (C) Similar to panel B, the import mixtures contained 0 or 3 μM GST-L. The cells were washed, fixed, and then visualized at the indicated times. The scale is the same as that described for panel B. (D) Similar to that shown in panel B, the import mixtures included the indicated concentrations of GST-L. −Cytosol, without added cytosol.

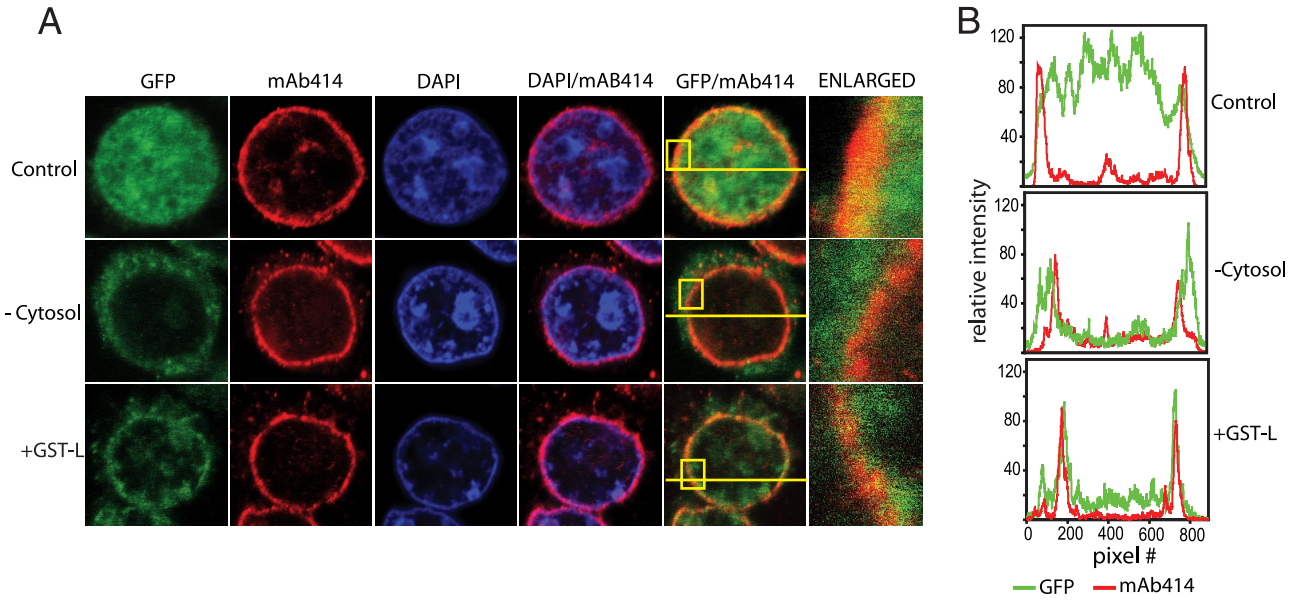

FIG. 4. Import cargo localization. (A) Digitonin-treated HeLa cells were reacted in GST-GFP$_{NLS}$ import assays as described in Fig. 3. After the cells were fixed, they were treated with DAPI and MAb 414 to label DNA and FG-containing NPC proteins, respectively. Imaging was performed as described in Materials and Methods. Boxes in the merged images (GFP/NPC) show the regions enlarged in the right-most panels. The lines show the scanned paths used to record the pixel density for individual data (color) channels. (B) The red (MAb 414) and green (GST-GFP$_{NLS}$) channel densities were plotted. All data were collected with identical image settings.

requirements for L-dependent activity could be measured by adding the effector(s) at the same time as the reporter. In this case, nuclear accumulation of added GST-GFP$_{NLS}$, not its loss, was the assay (Fig. 3A). Control samples, or those exposed to GST only, progressively accumulated nuclear fluorescence for at least 35 min at 20°C (Fig. 3C). When measured at this endpoint, GST-L-treated samples had nuclei visibly rimmed with reporter fluorescence, but the central nuclear signals were fivefold lower than those of controls (Fig. 3B). In reaction mixtures with WGA or without cytosol, the nuclear signals were reduced 30- and 10-fold, respectively, confirming that active import required functional NPCs as well as factors in the added cytosol. The added *Xenopus* extracts were the primary source of Ran, Ran cofactors, and cargo receptors. When tested for potency in these import assays, GST-L was most effective at micromolar concentrations, although high nanomolar levels still had some inhibitory activity (Fig. 3D). A time course at the 3 μM concentration for GST-L showed that the initial rate of reporter trafficking was unaffected for about the first 5 min of incubation (Fig. 3C). Thereafter, nuclear accumulation of additional fluorescence was impaired, suggesting a rapid L-dependent change to the NPC or, alternatively, a direct inhibition of one or more required import factors.

Import substrate localization. At low magnification, the patterns of GST-GFP$_{NLS}$ excluded from nuclei in the stalled import assays affected by GST-L or by the absence of cytosol appeared similar, suggesting that L was interfering with a step prior to docking of the NLS reporter at the NPC. But closer examination showed important differences in these patterns (Fig. 4A). Consistent with previous reports that the integrity of the NPC is not overtly altered by EMCV infection (20), staining with MAb 414, which recognizes FG repeat nucleoporins, as well as Nup62, Nup153, Nup214, and Nup358 (8) gave punctate nuclear rim stains in all samples, indicative of intact NPCs (Fig. 4A). The reproducibility of this stain was then used to mark and define the location of the nuclear envelope in cross-sectional scans with individual nuclei (Fig. 4B). Relative to the red channel (MAb 414), typical GFP fluorescence in control samples gave strong, uniform signals throughout the measured nuclei (e.g., top panel). As long as transport was active, the majority of the GFP was interior to and bounded by the red channel signals. With reactions carried out in the absence of added cytosol, only a small amount of GST-GFP$_{NLS}$ penetrated the nuclear interior. Retained traces of the green reporter signal (after washing and fixing) gave diffuse patterns outside the NPC rim. Treatment with GST-L also prevented nuclear accumulation of the reporter, but with these nuclei the residual GFP measurably concentrated into much sharper peaks which were generally congruent to the MAb 414 signals. Scanned nuclei from many cell fields in repeated experiments confirmed this basic pattern. When GST-L was present, some of the reporter cargo seemed to be partially imported, lodging within or near the NPC. The L protein appeared to block an import step during or immediately after docking of the cargo/receptor complex or its attempted transit through the NPC.

Nups are modified during EMCV infection. Since electron microscopy did not suggest a significant morphological breakdown of NPC during EMCV infection (20), it seemed prudent instead to look for chemical Nup changes that might account for altered permeability and/or failure of receptor-cargo complexes to achieve full, active import. Fractionation (SDS-PAGE) of cells over a time course of infection showed alterations in the banding patterns of several of the FG-nucleoporins reactive with MAb 414. In particular, Nup62 smeared upward on gels with a reproducible profile detectable as early as 2 h p.i. (Fig. 5A). The degree of Nup62 alteration increased

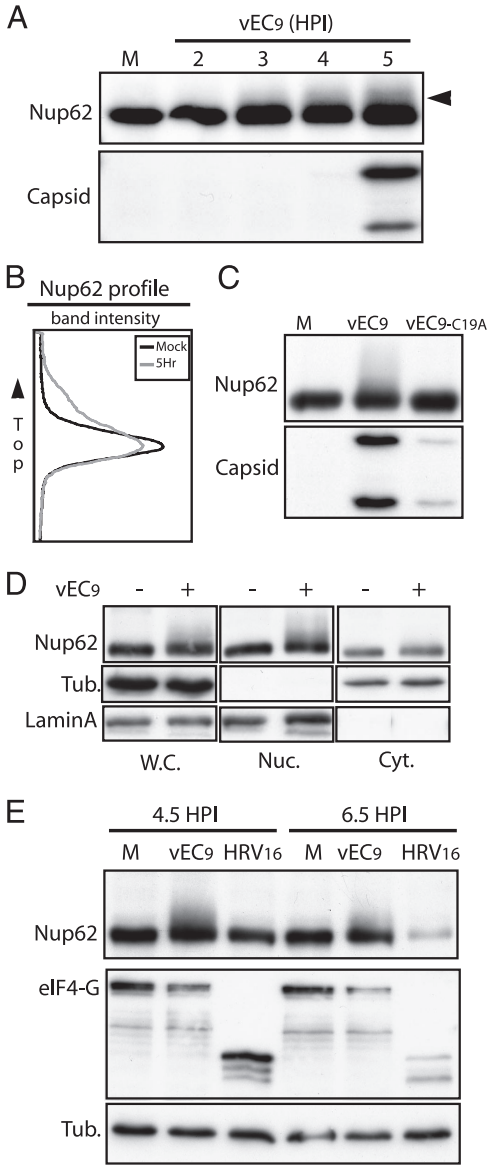

FIG. 5. Nup62 is modified during infection. (A) HeLa cells infected with vEC_9 (MOI = 50) were lysed in SDS at the indicated times p.i. Proteins were fractionated by PAGE and then visualized by Western blot analysis using MAb 414 or anti-EMCV antibody (Capsid). (B) The Nup62 bands for mock (M) and 5 h p.i. samples described for panel A were scanned and then plotted. (C) Infection and assays were performed as described for panel A (5 h p.i.), except the MOI was 5 (PFU) and one sample was infected with vEC_9-L_{C19A}. (D) Infection with vEC_9 was as described for panel A. At 4.5 h p.i., the cells were harvested and then fractionated (as described in Materials and Methods) into cytosolic (Cyt.), nuclear (Nuc.), or whole-cell (W.C.) extracts before PAGE and Western blot analyses were carried out. Tubulin (cytosol) and lamin A (nuclear) antibodies recorded the effectiveness of the cell fractionation techniques. (E) As described for panel A, cells were infected with vEC_9 or HRV-16 before being harvested at 4.5 or 6.5 h p.i. The tubulin bands provide gel loading controls. Cleavage of eIF4G is a positive control for effective HRV-16 infection.

in intensity between 2 and 5 h of infection, but the earliest protein shifts clearly preceded viral RNA replication (4 to 5 h p.i.) or significant capsid protein synthesis by at least 2 h. Scans of the protein bands showed that by 5 h p.i., about 25% of the Nup62 material (whole-cell extracts) was migrating more slowly (Fig. 5B). The mobility shift was not evident after infection with vEC_9-L_{C19A} virus harboring an inactive L protein (Fig. 5C). Although protein expression for this virus was reduced, the corresponding level of viral protein in wild-type-infected cells was sufficient to elicit the change in the Nup banding pattern. The altered Nup62 species were not evident in cytosol fractions from vEC_9-infected cells (Fig. 5D) or in whole-cell extracts prepared after infection with HRV-16 (Fig. 5E). The Nup mobility shift was specific to cells after wild-type EMCV infection and unique to those proteins isolated from nuclear fractions. That is, the shifted Nups were integral to the NPC. Since there was no detectable change in the overall distribution of nucleoporins during infection (Fig. 5D), the observed modification was not the cause or result of NPC disassembly.

Nup62 is a glycoprotein modified with O-linked *N*-acetylglucosamine residues and a known substrate for certain cellular kinases during the process of mitosis (21, 23). To determine which type of modification was triggered by EMCV, Nup62 was isolated by immunoprecipitation (MAb 414) from mock-infected or infected cells and then treated with alkaline phosphatase (Fig. 6A). The shifted forms from infected cells reverted to their original mobility, indicating that these species had been phosphorylated. In confirmation, parallel samples of nucleoporins isolated by immunoprecipitation (MAb 414 or control IgG) were fractionated by SDS-PAGE (Fig. 6B) and then probed with a phosphoprotein stain (Fig. 6C). When the gel was scanned and the sample lanes were superimposed (Fig. 6D), several trends were clear. All four FG repeat Nups, reactive with MAb 414, were measurably phosphorylated. Of these, only the phosphorylation status of Nup358 was unchanged by infection. A base level of phosphorylation was detectable for Nup214 and Nup153 in mock-infected cells, and these signals increased 40% and 20%, respectively, when the proteins were isolated from infected cells. For Nup62, the phospho stain (Fig. 6D) and parallel ^{32}P experiments (not shown) could not detect phosphorylation in mock-infected cells. But shortly after infection, the Nup62 phospho signal increased at least fivefold relative to baseline (mock MAb 414), the most dramatic peak change among the assayed Nups.

The parallel observation of nuclear efflux/import inhibition and Nup phosphorylation triggered by L strongly suggested that these phenomena were linked. If this was the case, recombinant GST-L should have triggered the same effect in our import assays in digitonin-treated cells (Fig. 7A). GST-L, but not WGA or GST, triggered rapid Nup phosphorylation, measured by Nup62 shift, at the same concentrations at which it inhibited import (3 μM to 300 nM) (Fig. 3D). It was unclear, however, whether Nup phosphorylation itself was the cause of trafficking inhibition or a downstream effect which perhaps resulted from the cessation of bidirectional transport triggered by some other L activity (e.g., Ran inhibition). To test this linkage, the GST-GFP_{NLS} import assays with digitonin-treated cells were repeated in the presence of staurosporine, a broad-spectrum kinase inhibitor (Fig. 7B to D). The drug rescued nuclear import from inhibition by GST-L but not from WGA, which prevents import by direct binding to glycosylated NPC components (Fig. 7B-C). The added staurosporine also blocked Nup phosphorylation, again measured by Nup62 as-

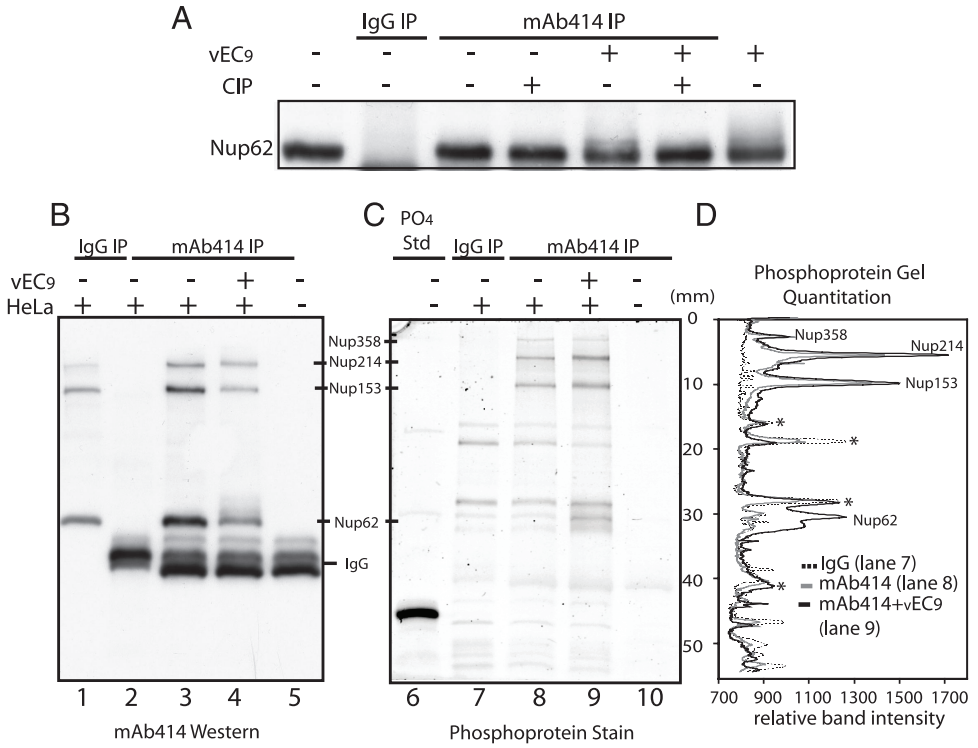

FIG. 6. Phosphorylation of FG nucleoporins. (A) Extracts from vEC_9- or mock-infected cells (4.5 h p.i.) were reacted with MAb 414 or IgG (control) in immunoprecipitation experiments (as described in Materials and Methods). Captured protein was treated with calf intestinal alkaline phosphatase before fractionation by PAGE and visualization by Western blot analysis (MAb 414). IgG immunoprecipitations from virus-infected and mock-infected cell lysates had identical patterns, and therefore the virus IgG control was not included in this figure. (B to D) Samples collected as described for panel A were fractionated on parallel gels by PAGE. (B) Band visualization was achieved by using Western blot analysis (MAb 414). (C) Band visualization was achieved by using the Pro-Q Diamond phosphoprotein stain. PO_4 Std, phosphoprotein reference standard. (D) Gel lanes in panel C corresponding with samples from vEC_9-infected cells immunoprecipitated with MAb 414 (mAb414 IP; solid black line; lane 9 in panel C), mock-infected cell samples immunoprecipitated with IgG (IgG IP; solid gray line; lane 7 in panel C), or MAb 414 (dashed black line; lane 8 in panel C) were scanned and plotted. Asterisks denote bands from the mock-infected cells which cross-reacted with both antibodies (i.e., background).

says, under the same conditions where GST-L was usually able to inhibit reporter trafficking (Fig. 7D). The correlation indicated that phosphorylation, presumably that of these Nups, was the most probable cause of L-dependent transport inhibition.

If the inhibitory mechanism was solely dependent on L-induced Nup phosphorylation, we surmised that treated nuclei, in the absence of L, would also demonstrate a defect in GST-GFP_{NLS} import. To test this hypothesis, permeabilized cells were incubated with cytosol containing L (or WGA control), washed to remove the effector-containing extracts, and then subjected to standard import reaction mixtures (cytosol plus GST-GFP_{NLS}). Pretreatment with L or WGA inhibited nuclear reporter accumulation to the same degree as in reactions where they were initially present in the cytosol (Fig. 8A and B). Subsequent protein analyses showed that these nuclei maintained the phosphorylated forms of Nup62 induced by exposure to L (Fig. 8C). These results confirmed that the phosphorylated Nups were the critical change in nucleocytoplasmic transport machinery leading to the L-dependent disruption in nucleocytoplasmic transport.

Required L protein domains. Several previous studies described EMCV L protein mutations that resulted in defective virus growth phenotypes in cell culture (6, 20, 38). Among these, $C_{19}A$ and $C_{22}A$ in the zinc finger domain and $T_{47}A$ in the acidic domain were reported to affect the trafficking inhibition induced by L protein (20). The T_{47} site and an additional Y_{41} site mutation (6) were also proposed to abrogate putative phosphorylation sites within L itself. A truncated L protein construct (Δa) removed these and extensive additional residues from the acidic domain. If the phosphorylation of L itself were contributing to the trafficking phenotypes, the effects should be recapitulated in cell-free assays. To test this idea, each mutant sequence (Fig. 9A) was reengineered into pGST-L, expressed in *E. coli*, and then purified as a recombinant protein. When assayed side-by-side against GST-L for their abilities to inhibit GST-GFP_{NLS} uptake into digitonin-treated HeLa cells, only GST-L_{C19A} was inactive (Fig. 9B). The GST-L_{Y41F}, GST-L_{T47A}, and GST-$L_{\Delta a}$ proteins behaved similarly to the wild-type protein and were very effective at inhibiting reporter uptake. Therefore, the L protein zinc finger alone was sufficient for this activity in cell-free assays, and L phosphorylation within the acidic domain (if it occurs) was not a requirement. Examination of the digitonin-treated nuclei after these reactions confirmed that in every case where reporter import was inhibited, nucleoporins (e.g., Nup62) became phosphorylated (Fig. 9C). A cytoplasmic factor was also clearly required for this activity, because none of the tested

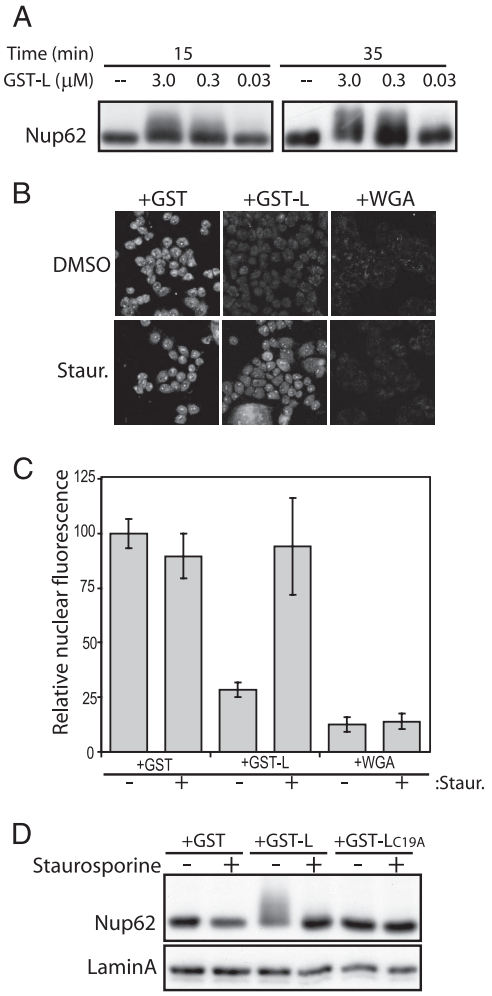

FIG. 7. Nucleoporin phosphorylation correlates with L activity. (A) Digitonin-treated HeLa cells were incubated with import mixtures containing GST-L at concentrations from 0.03 to 3.0 μM. After 15 or 35 min, washed cells were harvested in SDS, fractionated by PAGE, and analyzed by Western blot analysis. Nup62 was detected with MAb 414. (B) Digitonin-treated HeLa cells were incubated with import mixtures (as described in the legend to Fig. 3), which included GST-GFP_{NLS}, the indicated effectors (3 μM), and either dimethyl sulfoxide (DMSO) or 1 μM staurosporine (Staur.). After 35 min, the cells were washed, fixed, and visualized by confocal microscopy. (C) As described in the legend to Fig. 3, digitally captured confocal images of the GFP-specific pixels from 20 nuclei were recorded. The average pixel density (relative nuclear fluorescence) for the GST without staurosporine (control) was set at 100%. (D) Similar to panel B, digitonin-treated HeLa cells were incubated with import mixtures containing the indicated effectors (3 μM) and either DMSO (−) or 1 μM staurosporine (+). Washed cells were harvested in SDS, fractionated by PAGE, and analyzed by Western blot analysis. Nup62 was detected as described in panel A. Lamin A was the sample loading control.

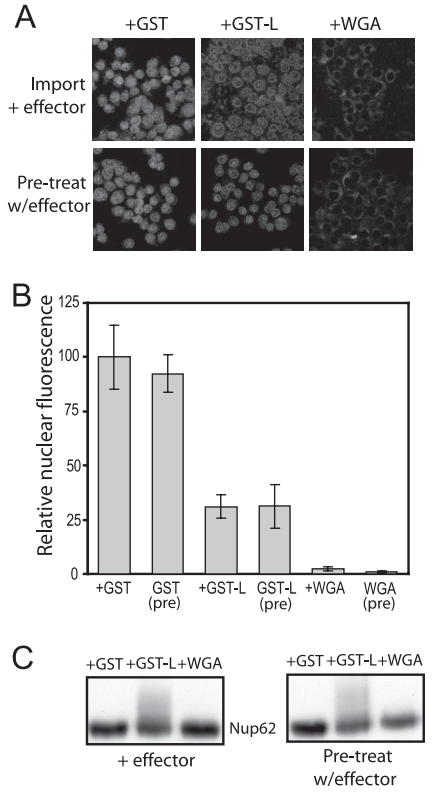

FIG. 8. Pretreatment with L protein inhibits import. (A) Digitonin-treated HeLa cells were incubated with an import mixture containing *Xenopus* egg cytosol, ATP, GTP with or without the indicated effector (3 μM GST, GST-L) or WGA control but lacking import substrate (GST-GFP_{NLS}). Cells were washed twice and then exposed to fresh import mixture with the reporter (GST-GFP_{NLS}) in the absence of the effector. Control reaction mixtures where the effector was added during import (Pre-treat w/effector; as described in the legend to Fig. 3) were prepared in parallel. The cells were washed, fixed, and then visualized by confocal microscopy. (B) As described in the legend to Fig. 3, digitally captured confocal images of the GFP-specific pixels from 20 nuclei were recorded. The average pixel density (relative nuclear fluorescence) for the GST (control) was set at 100%. (C) Digitonin-treated cells incubated with effectors as described in panel A were washed and harvested for Western blot analysis with MAb 414.

proteins were as effective when exogenous cytosol (from *Xenopus* eggs or HeLa cells) was omitted, even if ATP and GTP were included in the reaction buffers. The slight Nup62 shift observed in some of these treatments was likely due to incomplete removal of the endogenous cytoplasmic enzyme prior to the addition of recombinant protein.

Since our previous work mapped the disruption of Ran GTPase activity to an interaction with the L protein zinc finger domain, we tested whether the addition of saturating concentrations of recombinant human Ran would inhibit L-induced Nup phosphorylation. Even when added at a sixfold molar excess, Ran failed to alter the Nup phosphorylation pattern (Fig. 10), suggesting that the phenomenon was not directly related to titration of this essential transport factor.

DISCUSSION

The L proteins of cardioviruses are without homologues in sequence databases. The N-terminal CHCC zinc finger has a novel fold (4), and in the C-terminal portion, 14 of 31 residues are Asp or Glu, leaving the total protein (EMCV) with a pI of 3.8. Introduction of L into cells by infection, transfection of cDNA, or recombinant protein addition after cell permeabilization led to rapid cessation of active nucleocytoplasmic transport. Reporter proteins with NLS signals like GFP_{NLS} fail to import (Fig. 2 and 3), cellular mRNAs fail to export (30), and

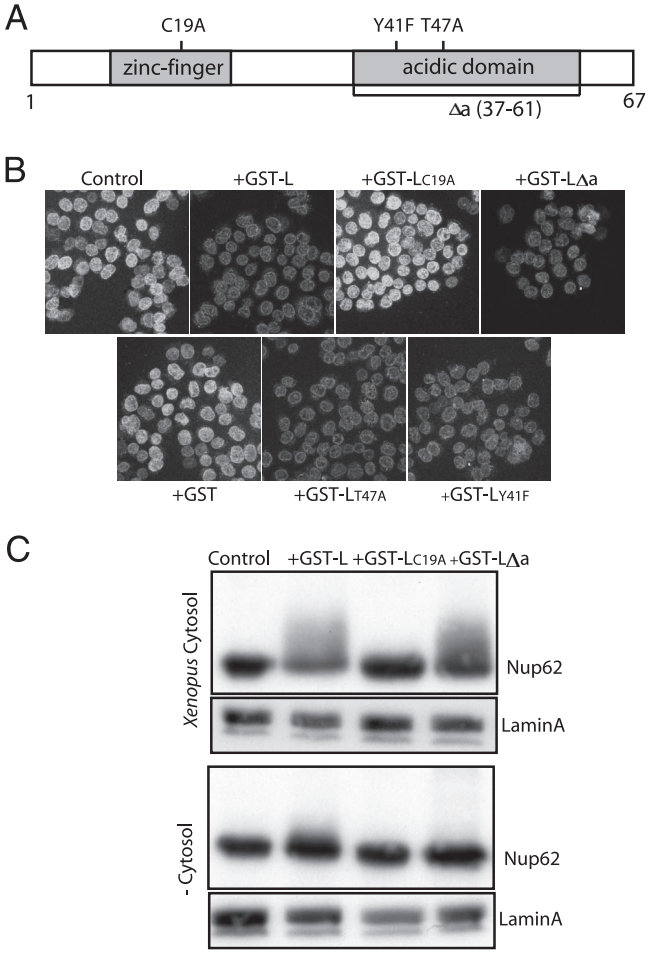

FIG. 9. Required L protein domains. (A) Mutational map of EMCV L recombinant proteins. (B) Digitonin-treated HeLa cells were incubated with import mixtures (as described in legend to Fig. 3), including GST-GFP_{NLS}, and indicated effectors (3 μM). After 35 min, the cells were washed, fixed, and visualized by confocal microscopy. (C) Digitonin-treated HeLa cells, as described in panel B, were incubated with the indicated effectors (3 μM) and ATP/GTP in the presence or absence of cytosol (from *Xenopus* eggs). Cells were washed, harvested in SDS, fractionated by PAGE, and analyzed by Western blot analysis (MAb 414 or lamin).

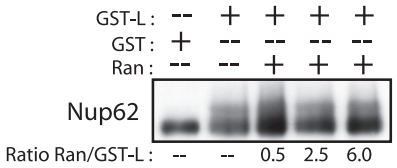

FIG. 10. The addition of Ran does not block L-induced nucleoporin phosphorylation. Digitonin-treated HeLa cells were incubated with import mixtures containing GST-L or the GST control protein (3.0 μM). Purified recombinant His_6-tagged Ran was added to the reaction mixtures at concentrations from 1.5 to 18 μM. After 35 min, treated cells were harvested in SDS, fractionated by PAGE, and analyzed by Western blotting. Nup62 was detected with MAb 414.

L-treated nuclei fail to retain GFP_{NLS}, HaloTag, or other proteins small enough for diffusion (20) (Fig. 1). In our assays with digitonin-treated cells, recombinant EMCV L, or, more precisely, the zinc finger domain of L protein, was the only viral protein motif required to recapitulate import inhibition or the unregulated efflux of nuclear-targeted proteins. Recombinant L proteins which lacked the acidic domain (Δa) or had mutations in either of the putative L phosphorylation sites (Y_{41} and T_{47}) had activities similar to those of wild-type L in these cell-free reaction mixtures (Fig. 9). It has been reported that EMCVs with the same mutations (Δa and $T_{47}A$) have reduced growth phenotypes during infection (6, 38), perhaps indicating that L takes part in multiple vital functions when introduced in a viral context. Our own growth studies with EMCV confirmed these observations (data not shown). However, the L effect on nucleocytoplasmic trafficking in cell-free assays was dependent only on a suitable reporter, nuclei, and the presence of an added cytosolic fraction, suggesting that L inhibitory activity is derived from a direct interaction of the zinc finger domain with one or more cellular partners.

Among the obvious cellular targets, we have reported that recombinant EMCV L binds tightly to recombinant Ran-GTPase and inhibits Ran GTP/GDP cycling activities in cell extracts (30). Ran is a very abundant protein in cells (12), and indeed our GFP_{NLS} import assays gave maximum L-dependent inhibition at micromolar concentrations sufficient to have titrated most Ran from the extracts. However, infected cells and especially early infected cells unquestionably have much more Ran than L. Our HaloTag assays measured nuclear efflux as early as 2 to 3 h after EMCV infection (Fig. 1). This means L or L-Ran complexes need to additionally leverage their inhibitory effects to abrogate most or all NPC activity within a short timeframe p.i. We believe that the L-triggered phenomenon which parallels Ran binding is the phosphorylation of core nucleoporins crucial to trafficking mechanisms. In every positive inhibition assay with cells or extracts, our antibodies detected that three FG repeat nucleoporins, Nup62, Nup153, and Nup214, were reproducibly hyperphosphorylated in an L-dependent manner. L sequences with inactivating mutations ($C_{19}A$) did not trigger this effect, nor did infection with another picornavirus (HRV-16) (Fig. 5E). When staurosporine, a broad-spectrum kinase inhibitor, prevented Nup phosphorylation, L was unable to inhibit nuclear trafficking (Fig. 7). In further support of this linkage, nuclei with NPCs phosphorylated by pretreatment with L remained defective in subsequent import reaction mixtures lacking the viral protein (Fig. 8).

FG repeat nucleoporins are displayed across the entire span of the NPC (36). During active transport, receptor-cargo complexes interact with the natively disordered repeat domains, facilitating movement across the pore (32). FG nucleoporins also interact within the NPC to maintain pore integrity and help form a barrier that is impermeable to passive diffusion (18, 28, 35). Certainly, phosphorylation of one or more Nups could interfere with the binding of cargo-receptor complexes or disrupt NPC self-interactions. Our assays focused on Nup62, as it is the target with the most visible gel shift phenotype and a key transport unit in the NPC central channel. The upward smear of this band, reversed by phosphatase treatment and reactive with phosphoprotein staining, predicts several L-dependent phosphorylation events per protein. The intensity of the shift increased over the course of EMCV infection (Fig. 5A), occurred only under conditions of L-induced import inhibition (Fig. 7 to 9), and coincided temporally with the onset

of nuclear efflux in cells or digitonin-treated nuclei. Since our Nup assays were necessarily defined by available antibodies (e.g., MAb 414), we cannot preclude that additional L-dependent Nup modifications occur in other NPC proteins. We are currently examining this possibility. It is probably not a coincidence, however, that viruses from the related *Enterovirus* genus of picornaviruses achieve trafficking inhibition by targeting their viral 2A protease to the NPC where they cleave the same Nup proteins we detected as being phosphorylated, thereby destroying the central NPC transport channel (3, 14, 27). Nup62 and Nup153 in particular are among the key substrates for these enzymes, suggesting that these core FG proteins are critical targets for picornavirus-induced regulation of NPC function (14, 15).

Cardiovirus L protein is not a kinase nor is its binding partner Ran. Phosphorylation is known to regulate nucleocytoplasmic trafficking by masking or unmasking localization signals on target proteins (29), but the contribution of nucleoporin phosphorylation to NPC function is understood only poorly. To be sure, during mitosis, cyclin-dependent kinases direct general modification of certain nucleoporins, causing the NPC to dissociate into subcomplexes that reside in the cytoplasm until the nuclear envelope is reassembled later in the cycle (22). Our results suggest that EMCV-induced Nup phosphorylation is not the result of an aberrant cyclin-dependent kinase activation. The collection of FG repeat proteins acted upon during infection is different than that targeted during mitosis (Nup153, Nup214, and Nup358) (8, 21, 23), and there is no evidence that NPCs are disassembled. The L-dependent phosphorylated form of Nup62 was retained in its entirety in the nuclear fraction of infected cells, and immunostaining patterns of other NPC proteins were unaltered by L. Moreover, unlike staurosporine, preliminary experiments with cyclin-dependent kinase inhibitors had no effect on EMCV-induced phosphorylation (F. W. Porter, unpublished data). Our data do suggest that the responsible kinase (or kinases) must be cytoplasmic, because L-dependent inhibition was never observed in the digitonin assays unless cytosolic extracts were included (Fig. 3). Infected HeLa cells and cell-free assays with *Xenopus* egg cytosol produced identical patterns, indicating that the requisite kinase(s) is ubiquitous and probably well conserved in eukaryotes.

We are in the process of characterizing the modified Nups and working with extensive panels of kinase inhibitors to identify the culpable cellular enzymes. It is unknown at this point whether L or L-Ran complexes provide the phosphorylation trigger. But some data do suggest that L-Ran binding is not coincidental to Nup phosphorylation. The isolated zinc finger domain of L was required and sufficient for inhibiting Ran activity in mitotic extracts (30), for triggering Nup62 phosphorylation in digitonin assays, for preventing active nuclear import of GFP_{NLS}, and for triggering unregulated nuclear efflux in cells and cell extracts. Staurosporine does not rescue microtubule aster formation in the presence of L, indicating that our reported results with Ran activity assays were not due to an L-induced kinase (unpublished data). The addition of a molar excess of recombinant Ran to our digitonin assays was likewise unable to rescue Nups from L-induced phosphorylation, suggesting that the mechanism is not the result of simple titration of the available protein (Fig. 10). We hypothesize that L or an L-Ran complex activates a normally quiescent cellular kinase or retargets a constitutively active kinase to phosphorylate the nucleoporins. As we work through the specifics of these mechanisms, we hope to verify the remarkably novel ways used by viruses to subvert common pathways and use them against the cell.

ACKNOWLEDGMENTS

We thank Christiane Wiese and Lori O'Brien for the generous gift of the *Xenopus* egg cytosol, Wai-Ming Lee for supplying the HRV-16, and Marchel Hill and Ewing Teen for their excellent technical help.

This work was supported by National Institutes of Health grant AI017331 to A.C.P. and a UW Biochemistry Department Scholar Fellowship to F.W.P.

REFERENCES

1. **Adam, S. A., R. S. Marr, and L. Gerace.** 1990. Nuclear protein import in permeabilized mammalian cells requires soluble cytoplasmic factors. J. Cell Biol. **111:**807–816.
2. **Aminev, A. G., S. P. Amineva, and A. C. Palmenberg.** 2003. Encephalomyocarditis virus (EMCV) proteins 2A and 3BCD localize to nuclei and inhibit cellular mRNA transcription but not rRNA transcription. Virus Res. **95:**59–73.
3. **Belov, G. A., P. V. Lidsky, O. V. Mitkitas, D. Egger, K. A. Lukyanov, K. Bienz, and V. Agol.** 2004. Bidirectional increase in permeability of nuclear envelope upon poliovirus infection and accompanying alterations of nuclear pores. J. Virol. **78:**10166–10177.
4. **Cornilescu, C. C., F. W. Porter, Q. Zhao, A. C. Palmenberg, and J. L. Markley.** 2008. NMR structure of the mengovirus Leader protein zinc-finger domain. FEBS Lett. **582:**896–900.
5. **Delhaye, S., V. van Pesch, and T. Michiels.** 2004. The leader protein of Theiler's virus interferes with nucleocytoplasmic trafficking of cellular proteins. J. Virol. **78**:4357–4362.
6. **Dvorak, C. M. T., D. J. Hall, M. Hill, M. Riddle, A. Pranter, J. Dillman, M. Deibel, and A. C. Palmenberg.** 2001. Leader protein of encephalomyocarditis virus binds zinc, is phosphorylated during viral infection and affects the efficiency of genome translation. Virology **290:**261–271.
7. **Faria, P. A., P. Chakraborty, A. Levay, G. N. Barber, H. J. Ezelle, J. Enninga, C. Arana, J. van Deursen, and B. M. Fontoura.** 2005. VSV disrupts the Rae1/mrnp41 mRNA nuclear export pathway. Mol. Cell **17:**93–102.
8. **Favreau, C., H. J. Worman, R. W. Wozniak, T. Frappier, and J. C. Courvalin.** 1996. Cell cycle-dependent phosphorylation of nucleoporins and nuclear pore membrane protein Gp210. Biochemistry **35:**8035–8044.
9. **Finlay, D. R., D. D. Newmeyer, T. M. Price, and D. J. Forbes.** 1987. Inhibition of in vitro nuclear transport by a lectin that binds to nuclear pores. J. Cell Biol. **104:**189–200.
10. **Fornerod, M., M. Ohno, M. Yoshida, and I. W. Mattaj.** 1997. Crm1 is an export receptor for leucine-rich nuclear export signals. Cell **90:**1051–1060.
11. **Görlich, D., and U. Kutay.** 1999. Transport between the cell nucleus and the cytoplasm. Annu. Rev. Cell Dev. Biol. **15:**607–660.
12. **Görlich, D., N. Pante, U. Kutay, U. Aebi, and F. R. Bischoff.** 1996. Identification of different roles for RanGDP and RanGTP in nuclear protein import. EMBO J. **15:**5584–5594.
13. **Gustin, K. E.** 2003. Inhibition of nucleo-cytoplasmic trafficking by RNA viruses: targeting the nuclear pore complex. Virus Res. **95:**35–44.
14. **Gustin, K. E., and P. Sarnow.** 2001. Effects of poliovirus infection on nucleocytoplasmic trafficking and nuclear pore complex composition. EMBO J. **20:**240–249.
15. **Gustin, K. E., and P. Sarnow.** 2002. Inhibition of nuclear import and alteration of nuclear pore complex composition by rhinovirus. J. Virol. **76:**8787–8796.
16. **Hahn, H., and A. C. Palmenberg.** 1995. Encephalomyocarditis viruses with short poly(C) tracts are more virulent than their mengovirus counterparts. J. Virol. **69:**2697–2699.
17. **Her, L.-S., E. Lund, and J. E. Dahlberg.** 1997. Inhibition of Ran guanosine triphosphatase-dependent nuclear transport by the matrix protein of vesicular stomatitis virus. Science **276:**1845–1848.
18. **Hu, T., T. Guan, and L. Gerace.** 1996. Molecular and functional characterization of the p62 complex, an assembly of nuclear pore complex glycoproteins. J. Cell Biol. **134:**589–601.
19. **Kalderon, D., W. D. Richardson, A. F. Markham, and A. E. Smith.** 1984. Sequence requirements for nuclear localization of simian virus 40 large T antigen. Nature **311:**33–38.
20. **Lidsky, P. L., S. Hato, M. V. Bardina, A. G. Aminev, A. C. Palmenberg, E. V. Sheval, V. Y. Polyakov, F. J. van Kuppeveld, and V. Agol.** 2006. Nucleocytoplasmic traffic disorder induced by cardioviruses. J. Virol. **80:**2705–2717.

21. **Macaulay, C., E. Meier, and D. Forbes.** 1995. Differential mitotic phosphorylation of proteins of the nuclear pore complex. J. Biol. Chem. **270:**254–262.
22. **Margalit, A., S. Vlcek, Y. Gruenbaum, and R. Foisner.** 2005. Breaking and making the nuclear envelope. J. Cell. Biochem. **95:**454–465.
23. **Miller, M. W., M. R. Caracciolo, W. K. Berlin, and J. A. Hanover.** 1999. Phosphorylation and glycosylation of nucleoporins. Arch. Biochem. Biophys. **367:**51–60.
24. **Moore, M. S., and E. D. Schwoebel.** 2000. Nuclear import in digitonin-permeabilized cells: current protocols in cell biology. John Wiley & Sons, New York, NY.
25. **Nakielny, S., and G. Dreyfuss.** 1999. Transport of proteins and RNAs in and out of nucleus. Cell **99:**677–690.
26. **Newmeyer, D. D., and K. L. Wilson.** 1991. Egg extracts for nuclear import and nuclear assembly reactions. Methods Cell Biol. **36:**607–634.
27. **Park, N., K. P., T. Skern, and K. E. Gustin.** 2008. Differential targeting of nuclear pore complex proteins in poliovirus-infected cells. J. Virol. **82:**1647–1655.
28. **Patel, S. S., B. J. Belmont, J. M. Sante, and M. F. Rexach.** 2007. Natively unfolded nucleoporins gate protein diffusion across the nuclear pore complex. Cell **129:**83–96.
29. **Poon, I. K., and D. A. Jans.** 2005. Regulation of nuclear transport: central role in development and transformation? Traffic **6:**173–186.
30. **Porter, F. W., Y. A. Bochkov, A. J. Albee, C. Wiese, and A. C. Palmenberg.** 2006. A picornavirus protein interacts with Ran GTPase and disrupts nucleocytoplasmic transport. Proc. Natl. Acad. Sci. USA **103:**12417–12422.
31. **Reichelt, R., A. Holzenburg, E. L. Buhle, M. Jarnik, A. Engel, and U. Aebi.** 1990. Correlation between structure and mass distribution of the nuclear pore complex and of distinct pore complex components. J. Cell Biol. **110**:883–894.
32. **Rexach, M., and G. Blobel.** 1995. Protein import into nuclei: association and dissociation reactions involving transport substrate, transport factors and nucleoporins. Cell **83:**683–692.
33. **Rout, M. P., J. D. Aitchison, A. Suprapto, K. Hjertaas, Y. Zhao, and B. T. Chait.** 2000. The yeast nuclear pore complex: composition, architecture, and transport mechanism. J. Cell Biol. **148:**635–652.
34. **Shah, S., S. Tugendreich, and D. Forbes.** 1998. Major binding sites for the nuclear import receptor are the internal nucleoporin Nup153 and the adjacent nuclear filament protein Tpr. J. Cell Biol. **141:**31–49.
35. **Stochaj, U., P. Banski, M. Kodiha, and N. Matusiewicz.** 2006. The N-terminal domain of the mammalian nucleoporin p62 interacts with other nucleoporins of the FXFG family during interphase. Exp. Cell Res. **312:**2490–2499.
36. **Tran, E., and S. Wente.** 2006. Dynamic nuclear pore complexes: life on the edge. Cell **125:**1041–1053.
37. **von Kobbe, C., J. M. van Deursen, J. P. Rodrigues, D. Sitterlin, A. Bachi, X. Wu, M. Wilm, M. Carmo-Fonseca, and E. Izaurralde.** 2000. Vesicular stomatitis virus matrix protein inhibits host cell gene expression by targeting the nucleoporin Nup98. Mol. Cell **6:**1243–1252.
38. **Zoll, J., W. J. Melchers, J. M. Galama, and F. J. van Kuppeveld.** 2002. The mengovirus leader protein suppresses alpha/beta interferon production by inhibition of the iron/ferritin-mediated activation of NF-κB. J. Virol. **76:**9664–9672.